Reprinted from JOURNAL OF APPLIED PHYSICS, Vol. 36, No. 2, 579-587, February, 1965

X-Ray Diffraction and Absorption Topography of Synthetic Diamonds*

Y. KAMIYA AND A. R. LANG
H. H. Wills Physics Laboratory, University of Bristol, Royal Fort, Bristol 8, England
(Received 28 August 1964)

Detailed observations were made on two selected GE synthetic diamonds; one was representative of the more perfect specimens, the other of less perfect but more common specimens. Diffraction topography of the more perfect crystal revealed lattice defects interpreted as dislocation bundles radiating from a central region, individual dislocations apparently resolvable locally, and a severely strained surface layer. Dislocations were not resolved in the less perfect specimen. Absorption topography using monochromatic Cu $K\alpha$ and Cu $K\beta$ radiations showed a nickel-rich surface film on the more perfect specimen, but few internal Ni-rich particles. The less perfect specimen contained many Ni-rich globules 2 to 15 μ in diameter, sheets of submicron-size Ni-impurity occluded under certain crystal edges and some Ni-rich surface film. The face-centered cubic "satellite" diffraction pattern of the less perfect specimen showed the presence of large crystallites misoriented up to 6° from the diamond matrix and fine crystallites closely parallel to the matrix. An explanation is put forward for the development of cube faces on synthetic diamonds.

1. INTRODUCTION

NATURAL diamonds have been the subject of more intensive scientific study than probably any other crystal found in nature, not least because of their striking variety in habit and other properties. This fact alone would attach interest to a study of the synthetic product. But the long duration of the struggle to make diamonds in the laboratory, the numerous early unsubstantiated claims of success, the sudden reversal of this unfortunate record by the development of an efficient synthesis process in the GE Research Laboratory,[1,2] all strengthen the interest in a thorough examination of the man-made specimens. The general morphology of synthetic diamonds has been described by Bovenkerk,[3] and numerous interferometric studies of their surfaces have been made by Tolansky.[4-6] Some of the chief differences in appearance between the natural and man-made stones are as follows: In the GE process for growing diamonds a thin film of molten metal "catalyst" separates the growing diamond from the reaction mixture. Dissolved carbon diffuses rapidly through this film to feed the growing crystals. The product often bears upon its faces an imprint resulting from the solidification of the "catalyst" film. The diamond surfaces are then veined and wrinkled in a manner not seen on natural stones. Another difference from natural stones is the occurrence of hoppered and skeletal growth, an understandable consequence of the faster growth rate. A more interesting and fundamental habit difference, however, is the frequent occurrence on synthetic diamonds of excellently smooth cube faces. Such faces are rare on natural stones, being found chiefly in specimens from the Congo, and are always extremely rough.

The x-ray diffraction patterns of synthetic diamonds have been thoroughly studied by Lonsdale, Milledge, and co-workers.[7,8] Their most notable finding with GE diamonds was the presence of a "satellite" pattern due to a small proportion of a face-centered cubic nickel-rich phase in parallel orientation with the diamond matrix. This fcc phase has a lattice parameter of 3.539 Å, a value intermediate between that of diamond, 3.567 Å, and of pure nickel, 3.523 Å.

Natural diamonds may exhibit a wide range of lattice perfection. In better specimens x-ray topography can reveal individual dislocations[9,10] and determine their Burgers vectors.[11] Good long-range regularity of the crystal lattice can be maintained even with the presence of appreciable impurity concentrated in the form of the platelets that produce the anomalous "spike" x-ray reflections of type I diamonds.[12,13] In other specimens a dispersion of precipitates may be present, causing dislocations to be naturally "decorated."[14] Experience of the variety of diffraction effects found in x-ray topographic studies of natural diamonds provided a background for the study of man-made diamonds by similar techniques.

Our investigations had three main aims: (1), to compare the lattice perfection attained in synthetic diamonds with that observed in natural stones, (2) to study topographically the distribution of impurity in synthetic diamonds, and (3) to look for topographic evidence bearing on the different surface and habit

* Research supported by the Aerospace Research Laboratories, OAR, through the European Office of Aerospace Research (OAR), U. S. Air Force.

[1] F. P. Bundy, H. T. Hall, H. M. Strong, and R. H. Wentorf, Jr., Nature **176**, 51 (1955).
[2] H. P. Bovenkerk, F. P. Bundy, H. T. Hall, H. M. Strong, and R. H. Wentorf, Jr., Nature **184**, 1094 (1959).
[3] H. P. Bovenkerk in *Progress in Very High Pressure Research*, edited by F. P. Bundy, W. Hibbard, and H. M. Strong (John Wiley & Sons, Inc., New York, 1961), p. 58.
[4] S. Tolansky and I. Sunagawa, Nature **184**, 1526 (1959).
[5] S. Tolansky, Proc. Roy. Soc. (London) **A263**, 31 (1961).
[6] S. Tolansky, Proc. Roy. Soc. (London) **A270**, 443 (1962).
[7] H. J. Grenville-Wells and K. Lonsdale, Nature **181**, 758 (1958).
[8] K. Lonsdale, H. J. Milledge, and E. Nave, Mineral. Mag. (London) **32**, 185 (1959).
[9] F. C. Frank and A. R. Lang, Phil. Mag. **4**, 383 (1959).
[10] A. R. Lang, J. Appl. Phys. **30**, 1748 (1959).
[11] A. R. Lang, Proc. Roy. Soc. (London) **A278**, 234 (1964).
[12] K. Lonsdale and H. Smith, Nature **148**, 112 (1941).
[13] M. Takagi and A. R. Lang, Proc. Roy. Soc. (London) **A281**, 310 (1964).
[14] C. J. Shah and A. R. Lang, Mineral. Mag. (London) **33**, 594 (1963).

characteristics of synthetic compared with natural diamond. Although our studies were mainly of an exploratory type we have obtained definite information on all the above-mentioned topics. Our findings suggest that further diffraction and absorption topographic work on synthetic diamonds would be very profitable.

We did not study many stones; only four GE and two South African synthetic diamonds were examined topographically. An account of the best GE specimen and also of one much less perfect but more typical is given here. These two specimens adequately illustrate the principal topographic phenomena observed. For each stone we describe the x-ray diffraction and absorption experiments performed upon it. After discussion of these we elaborate some ideas suggested by the topographs concerning the origin of the cubic habit in synthetic diamonds.

2. EXPERIMENTAL METHOD

The lattice perfection of the synthetic diamonds was studied by the methods of "projection topographs," [15] and "section topographs." [16] Variation in blackness on the topograph image can be due either to "orientation contrast" or to "extinction contrast," or to both together. Orientation contrast arises from the mutual misorientation of parts of the specimen preventing them from simultaneously satisfying the Bragg condition with equal efficiency. It can be detected, and the range of misorientations measured, by taking a series of section or projection topographs with the crystal inclined at different angles to a well-collimated incident beam. Extinction contrast is found only in crystals which are at least locally (i.e., in domains some microns in extent) sufficiently perfect for definite phase relationships to be maintained between all the rays participating in Bragg reflection. The diffraction contrast exhibited by the good specimen described in Sec. 3 was practically all extinction contrast, whereas the poorer specimen described in Sec. 4 showed both orientation and extinction contrast. Shorter x-ray wavelengths give stronger extinction contrast but, for various reasons, poorer topographic resolution. The expected and observed image widths of individual dislocations on diamond topographs, and other diffraction effects found in topographs of this crystal, have recently been discussed.[17] The first x-ray topographs of synthetic diamonds were made in 1959 using Mo $K\alpha$ radiation. The present diffraction experiments were all done with Cu $K\alpha$ radiation which allows a topographic resolution of about 1μ to be attained. Dislocation images in Cu $K\alpha$ topographs of natural diamonds are generally about 3–5 μ wide. Ilford L4 nuclear emulsion was used as the recording medium so that the contributions of emulsion grain size were negligible; any apparent granularity seen in the topographs arises from statistical fluctuations in image density. Stereopairs of projection topographs are helpful in locating internal defects; but with Cu $K\alpha$ radiation and the small interplanar spacings of diamond the high Bragg angles provide unnaturally large convergence angles for stereos.

Our absorption topographic experiments followed up the method used by Lonsdale, Milledge, and Nave[8] to establish the chemical identity of the fcc impurity phase. They compared the relative intensities of diamond and fcc satellite reflections produced by Cu $K\alpha$ and Cu $K\beta$ radiations on single-crystal rotation photographs. With Cu $K\beta$ radiation, which has a shorter wavelength than the nickel $K\alpha$ absorption edge, they found a marked weakening of the satellite reflections. This identified nickel as a major constituent of the impurity phase, and the degree of absorption loss of Cu $K\beta$ showed moreover that the impurity particles must be of order 5 μ in size. We have taken absorption topographs of our specimens using strictly monochromatic Cu $K\alpha$ and Cu $K\beta$ radiations. A parallel beam of uniform intensity was obtained through the 111 Bragg reflection of x rays from a highly perfect germanium crystal. During the exposure the germanium crystal was translated to and fro to provide a sufficiently broad and very uniform beam. The x-ray tube kilovoltage was kept below 24 kV so that the third harmonic wavelength would not be present in the reflected beam. The absorption topographs were, of course, on the same scale as the diffraction topographs, and the specimens were frequently set in approximately the same orientation as for Bragg reflection in order to facilitate correlation of features on diffraction and absorption topographs. The resolution on absorption topographs was at least equal to, and generally rather better than that on diffraction topographs. Nickel thicknesses of 5, 10, and 15 μ reduce the intensity of Cu $K\beta$ radiation to 0.27, 0.07, and 0.02 of its initial value, respectively. Thus nickel-rich inclusions of, say 7 μ in diameter and above are effectively quite opaque to Cu $K\beta$ radiation and stand out with extreme contrast. Nickel 15 μ thick and carbon 400 μ thick both reduce Cu $K\alpha$ to half its initial intensity, so that the larger nickel-rich inclusions are easily recognizable also on the Cu $K\alpha$ absorption topographs; and it follows too that their shadows can be seen on the Cu $K\alpha$ diffraction topographs, especially when the inclusions lie close to the x-ray exit surface of the specimen. Stereopairs of absorption topographs can be taken without the restriction that the specimen must make the Bragg angle with the incident rays. Thus the convergence angle can be chosen to produce the clearest depth visualization—an angle of 10° was found suitable.

The satellite diffraction pattern was studied by taking oscillation photographs of small angular range with the photographic plate sufficiently far from the specimen to separate the satellite reflections from those of the diamond. A plate distance of 11.4 cm was used for the 111

[15] A. R. Lang, Acta Cryst. **12**, 249 (1959).
[16] A. R. Lang, Acta Met. **5**, 358 (1957).
[17] F. C. Frank and A. R. Lang in *Physical Properties of Diamonds*, edited by R. Berman (Clarendon Press, Oxford, England, 1965), Chap. 3.

reflection and 5.4 cm for the higher-order reflections. Satellite reflections occurring together with allowed diamond reflections are superimposed on the Laue streak from the strong diamond reflection. This interference can be avoided by studying the satellite reflections of index 222 and 200. We used the latter in some of our experiments, since the diamond 200 "forbidden" reflection is extremely weak.

3. OBSERVATIONS ON A WELL-FORMED SPECIMEN

3.1. Morphology

We will describe first our experiments on a synthetic diamond which ranked among the most perfect of our specimens. Scale drawings of this crystal are shown in Fig. 1, diffraction topographs of it are reproduced in Figs. 2–6 and absorption topographs in Figs. 7 and 8. Like many synthetic diamonds this specimen is a macle (i.e., twin). The 111 twin plane divides the crystal into a major component, thickness 190 μ, and a minor component, thickness 60 μ. Figure 1(a) is a projection on to the twin plane. Continuous lines represent visible edges, interrupted lines are hidden edges (belonging to the minor component) and the chain line outlines the edges of the composition plane. Figure 1(b) is a view from the side and Fig. 1(c) a top view showing the location of three inclusions, A, B, and C. This crystal exhibited only two small cube faces. All surfaces of the crystal were rough. They showed no features characteristic of solution and appeared to be the final growth surfaces, a conclusion confirmed by x-ray studies. Although the crystal was transparent (color light yellow) the wrinkled surfaces made optical examination of the interior very difficult. This crystal showed relatively little birefringence, and most of it was concentrated in the vicinity of inclusions B and C.

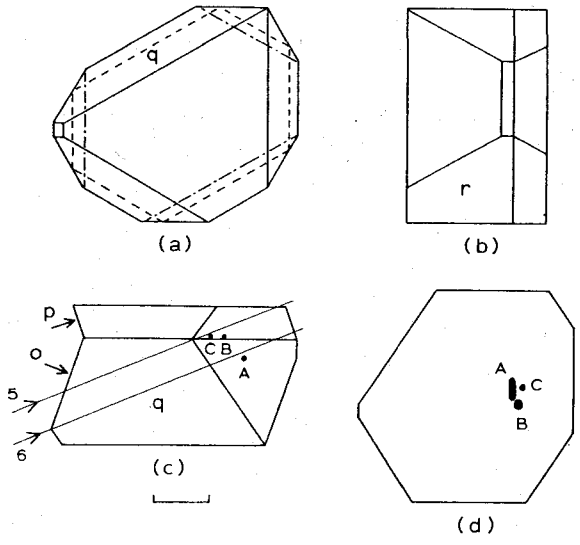

FIG. 1. Scale drawing of more perfect diamond twin, explained in text. Scale mark 100 μ.

FIG. 2. Projection topograph of synthetic diamond twin, twin plane reflection. Compare shape with Fig. 1(d). Scale mark 100 μ.

3.2. Diffraction Topography

Figure 2 is a projection topograph of the 111 reflection from the twin plane. Both components of the twin are reflecting and so the whole crystal contributes to the image. The shape of the image in Fig. 2 and of those in the other topographs shown of this crystal can be understood by reference to Fig. 1. Thus, Fig. 1(d) shows the outline of the crystal when viewed in a direction making the Bragg angle 22° with the twin plane, i.e., at an angle of view intermediate between those of Figs. 1(a) and (b). In fact the crystal was not mounted with an edge quite parallel to the goniometer axis, so that Fig. 2 is a little skewed with respect to Fig. 1(d). Much of the diffraction contrast in Fig. 2 comes from strained surface layers, particularly on the left-hand part of the image. However, one can discern within the crystal a general pattern of radiating lines of enhanced diffracting power and a broad column of imperfect crystal running upwards from the center of the specimen. Figure 3 is a projection topograph of the major component of the twin, obtained by Bragg reflection from planes parallel to the octahedral face marked o in Fig. 1(c). Contrast due to the strained surface is most evident in the marginal areas of this view of the crystal so that the radiating pattern of internal defects is less obscured. The rod-like inclusion A, the larger round inclusion B, and smaller round inclusion C produce faint shadows in Fig. 2 but are not seen in Fig. 3 since in the latter reflection most of the image-producing volume lies between them and the x-ray exit surface of the crystal. In Fig. 4, on the other hand, which is a projection topograph of the minor component of the twin taken by Bragg reflection from planes parallel to p, the shadows of the three inclusions are clear. This is because B and C lie in the twin-plane and A is imbedded in the major component, i.e., on the observer's side of the diffracting volume. Measurement of the relative positions of the shadows of A, B, and C in these and other topographs

FIG. 3. Projection topograph of major component of twin, reflection from planes parallel to o in Fig. 1(c).

enable their positions to be fixed within about $\pm 5\,\mu$. The reflection used in Fig. 4 has the advantage that the x-ray exit surface over most of the image area is the composition plane and not a strained outer crystal surface. Hence the internal defects show up well; most of them appear to radiate from the vicinity of the inclusions B and C. However, on the left-hand margin of this image extreme surface strain is evident, causing loss of reflection from one small region by misorientation.

The technique of "limited projection topographs," [18] in which the diffracted-beam slits are adjusted to prevent the unwanted images of surface damage reaching

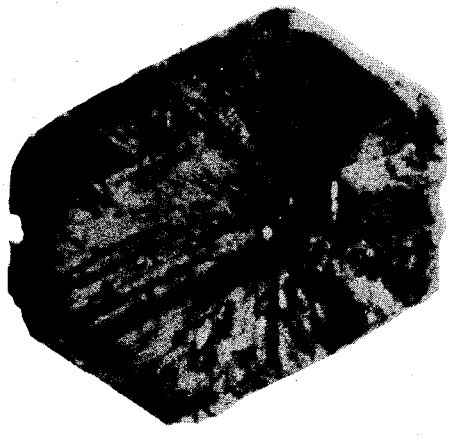

FIG. 4. Projection topograph of minor component of twin, reflection from planes parallel to p in Fig. 1(c).

the photographic emulsion, cannot conveniently be applied to such small crystals as now concern us, but the superimposition of the direct images of internal and surface defects is avoided in section topographs. Moreover, section topographs show higher diffraction contrast from individual defects than do projection topographs. Figures 5 and 6 are section topographs in which the incident x-ray beam (about 15 μ wide) cuts the specimen along the lines marked 5 and 6 in Fig. 1(c), using the twin-plane Bragg reflection. Section 5 cuts the crystal close to inclusions B and C; columns of defects fan out above and below these inclusions, individual lines fan out in all directions and surface strain is locally intense. Figure 6 is generally similar. This section cuts through several radiating columns but the inclusion A does not appear responsible for generating noticeable lattice defects; it lies to the right of the highly distorted central region cut by the section. Nor is there a concentration of defects in the twin plane which is intersected close to the right-hand margin of the image.

3.3. Absorption Topographs

Figures 7 and 8 show a stereopair of absorption topographs taken with Cu $K\beta$ radiation, the former with

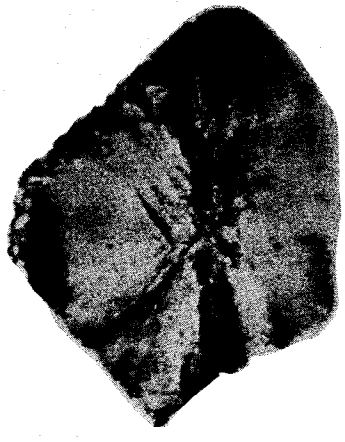

FIG. 5. Section topograph with incident beam cutting crystal along line 5, Fig. 1(c), twin plane reflection.

an angle of view making about 42° with the twin plane, and the latter 32°. The latter view of the crystal is thus roughly comparable with that of Figs. 1(d) and 2. The large internal inclusions A, B, and C are obvious. A number of small globular absorbing particles with diameters in the 2- to 5-μ range are also evident; stereo examination shows that they are concentrated at or near the surface. But the most striking feature is presented by Fig. 7. As already mentioned, the crystal was mounted slightly skew with respect to the orientation drawn in Fig. 1. This tilt brings the two octahedral faces

FIG. 6. Section topograph with incident beam cutting crystal along line 6, Fig. 1(c), twin plane reflection.

[18] A. R. Lang, Brit. J. Appl. Phys. 14, 904 (1963).

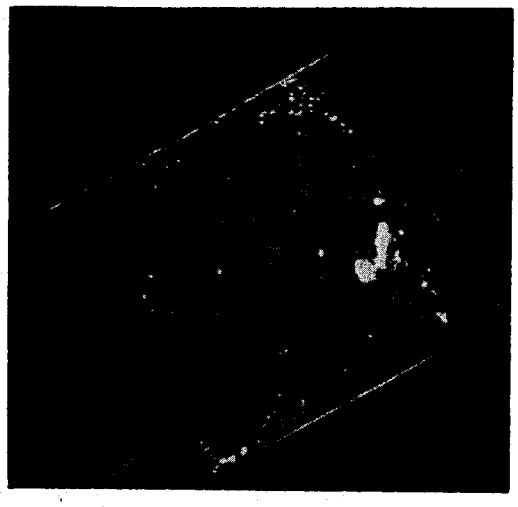

FIG. 7. Cu $K\beta$ absorption topograph, angle of view about 42° with twin plane of specimen drawn in Fig. 1.

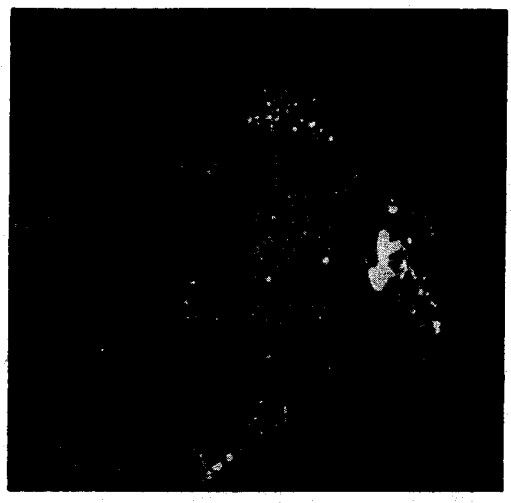

FIG. 8. Cu $K\beta$ absorption topograph, angle of view about 32° with twin plane of specimen drawn in Fig. 2.

q and r parallel to the x-ray beam in Fig. 7. Strong absorption contrast is produced by the surface skin on these faces, now seen edge-on. The ratio of absorption contrast shown in Cu $K\alpha$ and Cu $K\beta$ absorption topographs of this crystal is quite consistent, with nickel being the major absorbing constituent in the individually resolvable particles, with the exception of inclusion B which appears to absorb Cu $K\alpha$ more strongly than would pure nickel.

3.4. Satellite Diffraction Pattern

It is a reasonable assumption that these individually resolvable nickel-rich particles seen on absorption topographs give rise to the satellite reflections. Oscillation photographs of small angular range were taken about the 111 and 220 diamond reflections. No satellite spots were detected. It is possible that the major particles may have been missed in these experiments since the incident beam did not bathe the whole crystal, or that the satellite structures may have been appreciably misorientated from the crystal matrix. However, considering that in this specimen the estimated aggregate weight of nickel in individually resolvable particles is only about 0.02 μg, that is about 2×10^{-4} of the weight of diamond present, failure to observe the satellite reflections is understandable.

4. OBSERVATIONS ON A LESS PERFECT SPECIMEN

4.1. Morphology

Apart from its relatively large size, 0.5 mm, the specimen we will now describe was much more representative of synthetic diamonds in general. It was again a macle, consisting of two incomplete elongated octahedra joined together on the twin plane. Figure 9(a) is a view of the crystal corresponding roughly with those of the diffraction topograph Fig. 10 and the absorption topographs Figs. 11–13. The better developed faces are on the x-ray exit surface, nearer the observer. All other surfaces were quite irregular. The base was possibly a fracture surface. The surfaces far from the observer showed skeletal growth and were partly hollowed out. There was some evidence that solution had occurred. The crystal was opaque except for a few transparent patches close to some edges.

4.2. Diffraction Topographs

A number of projection topographs and section topographs taken of this specimen showed that the lattice perfection was greatly inferior to that of the specimen described in Sec. 3. Orientation contrast as well as extinction contrast contributed to the variation of density of the image; in parts of the specimen the orientation spread was of order 5′. The projection topograph Fig. 10 uses the twin plane reflection so that the whole crystal appears in the image. Intense concentrations of strain are seen in several regions, and lines of imperfection tend to run parallel with ⟨110⟩ directions. They appear related to the strings of inclusions in similar directions seen on the absorption topographs. We wish to draw attention to a sheet of imperfection running

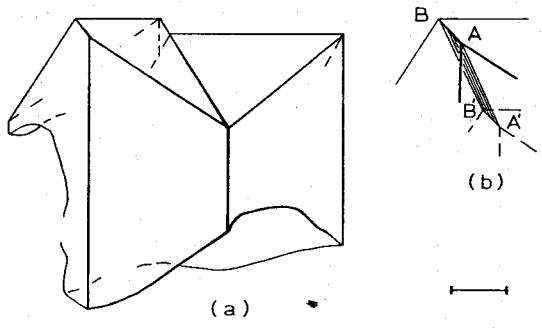

FIG. 9. (a) Shape of imperfect synthetic diamond twin as it appears in topographs Figs. 10–12, (b) location of sheet of occluded impurity ABB′A′ in top left corner of Fig. 9(a). Scale mark 100 μ.

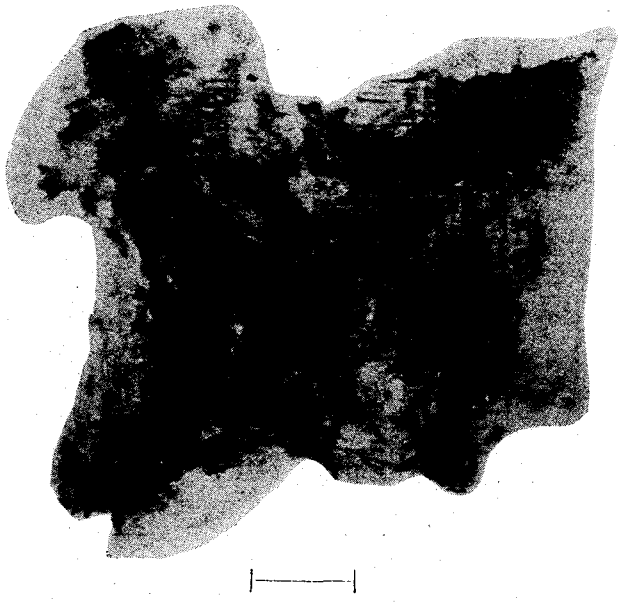

FIG. 10. Projection topograph of imperfect synthetic diamond twin, twin plane reflection. Scale mark 100μ.

down from the left-hand top corner of the image; this is further discussed below.

4.3. Absorption Topographs

Figures 11 and 12 are a stereopair of absorption topographs taken with Cu $K\beta$ radiation. A great number of absorbing particles is seen compared with the few shown in Figs. 7 and 8. The smaller individual particles appear generally globular, with diameters in a rather narrow size range, 2–7 μ. The larger particles appear to have been formed by the coalescence of strings of globules and they often lie parallel to ⟨110⟩ directions. Figures 11 and 12 are members of a series of absorption topographs taken at roughly 10° intervals, starting with the x rays parallel to the twin plane. Figure 11 is a left-eye view, making 32° with the twin plane. Figure 12 is the right-eye view, making the Bragg angle with the twin plane and thus corresponding to the projection topograph Fig. 10. The parallax between near and far inclusions is easily noticed in Figs. 11 and 12, but prints such as these cannot adequately portray the striking appearance of the original plates when examined under twin microscopes. The opaque inclusions then appear to be suspended around and within the nebulous form of the weakly absorbing diamond. Relative positions of the inclusions can be fixed accurately, and it is clear that most of them are at or very close to the crystal surface. The specimen was subjected to a 50-h etch in aqua regia and the absorption topographs repeated, *but none of the absorbing particles disappeared or detectably diminished in size through this treatment.* The more irregular surfaces of this specimen compared with that described in Sec. 3 would render an absorbing skin less readily detectable, but we found definite evidence for the presence of such a skin on some parts of its surface.

One might expect occlusion of impurity to occur at the re-entrant angles where the two components of the twin pair meet, but the absorption topograph taken with the x rays passing parallel to the twin plane gave no evidence of any extra absorbing material in the twin plane. The absorption topographs do show, however, that considerable occlusion of absorbing material has occurred elsewhere. The diffuse region of extra absorp-

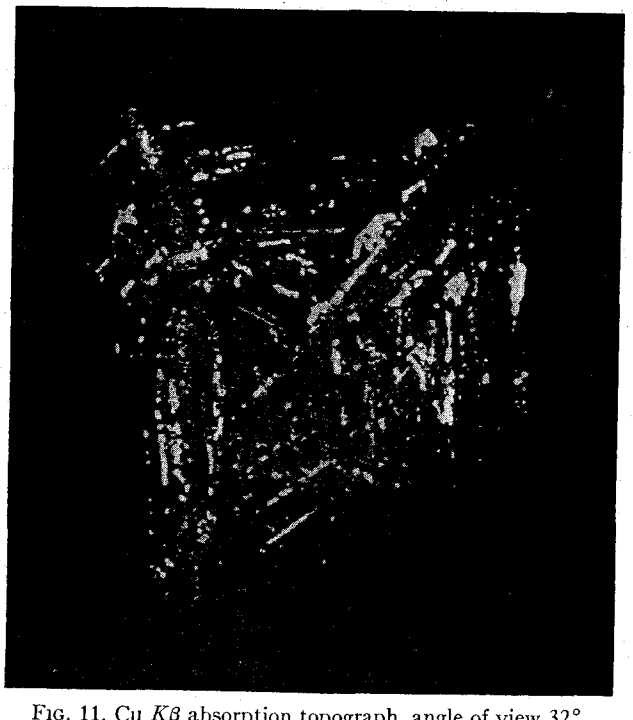

FIG. 11. Cu $K\beta$ absorption topograph, angle of view 32° with twin plane of imperfect specimen.

FIG. 12. Cu $K\beta$ absorption topograph, angle of view 22° with twin plane of imperfect specimen.